Fractional Fourier Transform-Based OFDM in LoS-Dominant Multi-Cluster NTN Channels: A Structural Analysis

Soo Young Shin, Senior Member, IEEE, and Victor C. M. Leung, Fellow, IEEE

***Abstract*—Fractional Fourier transform (FrFT)-based OFDM has been reported to improve banded equalization when channel energy is approximately aligned with a single FrFT-diagonal ridge. This letter examines that premise for a LoS-dominant multi-cluster non-terrestrial network (NTN) channel under a TR 38.811-inspired Ka-band parameter regime. A concise structural argument indicates that the optimal FrFT order tends to collapse to the DFT point when the line-of-sight (LoS) concentration loss caused by rotation exceeds the clustered-part concentration gain available in the FrFT domain. Synthetic-operator sanity tests verify that the discrete FrFT implementation and the order-selection rule recover non-DFT optima when such optima exist. Monte Carlo BER results indicate no measurable FrFT gain over FFT-OFDM across $\kappa \in \{1000, 1300, 1600\}$ Hz/sample and two geometry assumptions, while a slight penalty appears at narrow equalization bandwidths.**

***Index Terms*—Fractional Fourier transform, OFDM, non-terrestrial networks, banded equalization, delay–Doppler channels.**

I. Introduction

Non-terrestrial networks (NTNs), including low-earth-orbit satellites and high-altitude platform stations, operate under severe Doppler and delay variations that give rise to strongly doubly dispersive channels [1], [2]. In OFDM systems, such propagation yields dense effective channel matrices, which has motivated alternative transform domains for low-complexity equalization.

The fractional Fourier transform (FrFT) is of interest because it can concentrate channel energy near the diagonal when the underlying channel is approximately aligned with a single dominant chirp-like ridge [3]–[6]. Corresponding gains have mainly been reported in channels whose delay–Doppler support is effectively single-ridge, such as simplified underwater acoustic or visible-light settings [7], [8]. For LoS-dominant multi-cluster NTN channels, however, a single globally alignable ridge is generally not guaranteed.

The channel considered here follows a TR 38.811-inspired Ka-band NTN parameter regime while retaining a LoS-dominant multi-cluster LTV structure with cluster-dependent delay–Doppler slopes. Under this setting, the main question is not whether FrFT can outperform broader waveform families, but when FrFT-OFDM itself ceases to be effective. In particular, a null result in such a channel becomes structurally informative when the FrFT implementation is known to recover non-DFT optima on operators that are approximately diagonal in a single FrFT basis.

The main contributions are summarized as follows.

1) A structural criterion is derived for predicting when the optimal FrFT order collapses to the DFT point in LoS-dominant multi-cluster NTN channels, revealing that incompatible delay–Doppler slopes fundamentally limit the usefulness of a single global FrFT rotation.
2) Synthetic operators with known non-DFT optima verify that the discrete FrFT realization and order-selection rule recover non-DFT optima when they exist, ensuring that the reported null result reflects channel structure rather than numerical artifacts.
3) Monte Carlo BER results under amplified coupling stress and two geometry assumptions confirm no measurable FrFT gain over FFT-OFDM, with a slight penalty at narrow equalization bandwidths, clarifying that FrFT-OFDM benefit is contingent on whether the channel admits a single globally alignable ridge.

II. System Model

A. FrFT-OFDM with banded equalization

Let N denote the OFDM block length and let $\boldsymbol{s} \in \mathbb{C}^N$ be the transmitted QPSK symbol vector. In FrFT-OFDM, the time-domain transmit signal is

$$\boldsymbol{x} = \boldsymbol{F}_p^H \boldsymbol{s}, \tag{1}$$

where $\boldsymbol{F}_p \in \mathbb{C}^{N\times N}$ is the unitary discrete FrFT matrix of order p, with $p = 1$ reducing to the unitary DFT matrix $\boldsymbol{F}$. In the numerical implementation, $\boldsymbol{F}_p$ is constructed using a unitary discrete FrFT realization based on the eigendecomposition of the DFT operator [9].

After propagation through a linear time-varying (LTV) channel $\boldsymbol{H}$ and additive white Gaussian noise $\boldsymbol{w} \sim \mathcal{CN}(\boldsymbol{0}, \sigma^2\boldsymbol{I})$, the receiver applies the same transform order and obtains

$$\boldsymbol{r} = \boldsymbol{F}_p\boldsymbol{H}\boldsymbol{F}_p^H\boldsymbol{s} + \boldsymbol{F}_p\boldsymbol{w} \triangleq \boldsymbol{G}(p)\boldsymbol{s} + \boldsymbol{F}_p\boldsymbol{w}. \tag{2}$$

Only the $2Q+1$ circular diagonals of $\boldsymbol{G}(p)$ are retained, and the resulting banded LMMSE problem is solved by preconditioned conjugate gradient (PCG), where $Q \in \{0, 1, \ldots, 5\}$

S. Y. Shin is with the Dept. of IT Convergence Engineering, Kumoh National Institute of Technology, Gumi, Republic of Korea (e-mail: wdragon@kumoh.ac.kr). (Corresponding author: Soo Young Shin.)

V. C. M. Leung is with the Dept. of Electrical and Computer Engineering, The University of British Columbia, Vancouver, BC, Canada (e-mail: vleung@ece.ubc.ca).

denotes the half-bandwidth. This follows the standard low-complexity banded-equalization viewpoint for doubly selective OFDM channels [10], [11].

The FrFT order is selected offline and independently for each Q from a finite grid $\mathcal{P} = \{0.55, 0.57, \ldots, 1.55\}$. The order p*(Q) is selected by maximizing

$$p^\star(Q) = \arg\max_{p\in\mathcal{P}} J(p, Q), \tag{3}$$

where $J(p, Q)$ is the order-selection score averaged over M_{sel} pilot channel realizations. In the numerical results, the score is evaluated using a truncation-aware MSE surrogate at a fixed selection SNR of 20 dB.

B. LoS-dominant multi-cluster NTN channel

The channel considered here is an LTV model that follows the same TR 38.811-inspired Ka-band NTN parameter regime while including cluster-dependent delay–Doppler structure. The model is intended to represent a LoS-dominant multi-cluster NTN channel in which ridge-like coupling can arise locally, but a single globally compatible slope is not guaranteed. The channel matrix is written as

$$\boldsymbol{H} = \boldsymbol{H}_{\mathrm{LoS}} + \boldsymbol{H}_{\mathrm{dom}} + \boldsymbol{H}_{\mathrm{sec}} + \boldsymbol{H}_{\mathrm{bg}} + \boldsymbol{H}_{\mathrm{diff}}, \tag{4}$$

where the dominant and secondary clusters contain $L_{\mathrm{dom}} = 6$ and $L_{\mathrm{sec}} = 5$ sub-paths, respectively.

The physical parameters follow the Ka-band NTN setting; key values are listed in Table I. For a dominant sub-path ℓ, the initial Doppler is modeled as

$$\nu_\ell = \nu_0 + \kappa(\tau_\ell - \tau_{\mathrm{ref}}) + \delta\nu_\ell, \qquad \ell \in \mathrm{dom}, \tag{5}$$

where κ [Hz/sample] controls the ridge tilt and $\delta\nu_\ell$ is a per-path jitter term. A physical estimate of κ is obtained by expressing the delay-domain slope as $\kappa_{\mathrm{phys}} = \Delta\nu/\Delta\tau_{\mathrm{samp}}$, where $\Delta\nu$ [Hz] is the inter-path Doppler spread and $\Delta\tau_{\mathrm{samp}} = \tau_{\mathrm{DS}}/T_s$ [sample] is the delay spread expressed in sample units ($T_s = 1/(N\Delta f) \approx 260$ ns for the parameters in Table I). With $\tau_{\mathrm{DS}} = 550$ ns and $\Delta\nu$ estimated at 100–300 Hz—an order-of-magnitude figure consistent with the residual inter-path Doppler spread after beam-centric compensation at the Ka-band LEO operating point selected here [1]—this gives $\kappa_{\mathrm{phys}} \approx$ 400–600 Hz/sample. The values $\kappa \in \{1000, 1300, 1600\}$ Hz/sample are deliberately chosen above this physical range to provide amplified coupling stress conditions that increase the potential for FrFT concentration gain; a null result under these conditions is therefore a stronger negative finding than one obtained at physically expected coupling levels alone. The secondary cluster uses a reduced slope

$$\kappa_{\mathrm{sec}} = \zeta\kappa, \qquad \zeta = 0.55, \tag{6}$$

with either an independent reference delay (INDEP) or a shared reference delay (SHARED). Thus, even when the large-scale NTN parameters are fixed, the channel contains two incompatible effective slopes. This is the structural feature that challenges a single-order FrFT basis.

TABLE I
LoS-DOMINANT MULTI-CLUSTER NTN CHANNEL PARAMETERS

Parameter	Symbol	Value
Carrier frequency	f_c	20 GHz
Subcarrier spacing	Δf	15 kHz
Block length	N	256
Platform velocity	v	7500 m/s
Delay spread	τ_{DS}	550 ns
Half-bandwidth	Q	$0, 1, \ldots, 5$
Selection realizations	M_{sel}	60
BER realizations	M	10,000
Ridge tilt	κ	1000, 1300, 1600 Hz/sample
Secondary slope ratio	ζ	0.55
Dominant cluster power	P_{dom}	-8 dB
Secondary cluster power	P_{sec}	-15 dB

III. Structural Analysis

A. Why the optimal order tends to collapse to $p^\star = 1$

Write the channel as

$$\boldsymbol{H} = \boldsymbol{H}_{\mathrm{LoS}} + \boldsymbol{H}_{\mathrm{cl}}, \tag{7}$$

where

$$\boldsymbol{H}_{\mathrm{cl}} \triangleq \boldsymbol{H}_{\mathrm{dom}} + \boldsymbol{H}_{\mathrm{sec}} + \boldsymbol{H}_{\mathrm{bg}} + \boldsymbol{H}_{\mathrm{diff}}. \tag{8}$$

Because $\boldsymbol{G}(p) = \boldsymbol{F}_p \boldsymbol{H} \boldsymbol{F}_p^H$, the order-selection score may be interpreted as a competition between a LoS-driven term and a clustered term:

$$J(p, Q) \approx \alpha J_{\mathrm{LoS}}(p, Q) + (1 - \alpha) J_{\mathrm{cl}}(p, Q), \tag{9}$$

where $\alpha = P_{\mathrm{LoS}}/(P_{\mathrm{LoS}} + P_{\mathrm{cl}})$ is the LoS power fraction. The approximation in (9) holds under two conditions satisfied by the channel considered here. First, the LoS power dominates the clustered power ($\alpha \approx 0.909$, i.e. $P_{\mathrm{LoS}}/P_{\mathrm{cl}} \approx 10$). Since $\|\boldsymbol{G}_{\mathrm{cl}}\|_F/\|\boldsymbol{G}_{\mathrm{LoS}}\|_F \approx \sqrt{P_{\mathrm{cl}}/P_{\mathrm{LoS}}} \approx 0.32$, the cross-term between $\boldsymbol{G}_{\mathrm{LoS}}(p)$ and $\boldsymbol{G}_{\mathrm{cl}}(p)$ is treated as secondary relative to the LoS term in any single realization, and is further suppressed in expectation by the second condition below. Second, the cluster sub-path gains are modeled as independent zero-mean complex Gaussian random variables, so the expected cross-term satisfies $\mathbb{E}[\langle \boldsymbol{G}_{\mathrm{LoS}}(p), \boldsymbol{G}_{\mathrm{cl}}(p)\rangle_F] = 0$, and vanishes under the Monte Carlo average.

The LoS component is maximized at the DFT point $p = 1$. Let

$$\boldsymbol{H}_{\mathrm{LoS}} = a_0 e^{j\phi} \boldsymbol{D}(\nu_0), \qquad \boldsymbol{D}(\nu_0) = \mathrm{diag}\big(e^{j2\pi\nu_0 n T_s}\big). \tag{10}$$

Then, at $p = 1$,

$$\boldsymbol{F}\boldsymbol{H}_{\mathrm{LoS}}\boldsymbol{F}^H = a_0 e^{j\phi} \boldsymbol{F}\boldsymbol{D}(\nu_0)\boldsymbol{F}^H = a_0 e^{j\phi} \boldsymbol{P}_{\nu_0}, \tag{11}$$

where $\boldsymbol{P}_{\nu_0}$ is a circular-shift permutation matrix. Hence all LoS energy lies on a single circular diagonal, which yields

$$J_{\mathrm{LoS}}(1, Q) = 1, \qquad Q \geq 0. \tag{12}$$

For $p \neq 1$, the matrix $\boldsymbol{F}_p \boldsymbol{D}(\nu_0) \boldsymbol{F}_p^H$ is no longer a permutation, and its energy spreads over multiple diagonals. This implies that

$$J_{\mathrm{LoS}}(p, Q) < 1. \tag{13}$$

A non-DFT order can therefore be helpful only when the clustered component provides enough additional concentration to offset the LoS loss. Define

$$\Delta J_{\mathrm{cl}}(Q) \triangleq \max_{p} J_{\mathrm{cl}}(p,Q) - J_{\mathrm{cl}}(1,Q), \tag{14}$$

and

$$\Delta J_{\mathrm{LoS}}(Q) \triangleq J_{\mathrm{LoS}}(1,Q) - \min_{p} J_{\mathrm{LoS}}(p,Q). \tag{15}$$

Then the DFT point remains optimal whenever

$$\alpha > \alpha_{\mathrm{th}}(Q) \triangleq 1 - \frac{\Delta J_{\mathrm{cl}}(Q)}{\Delta J_{\mathrm{LoS}}(Q)}. \tag{16}$$

Equation (16) serves here as an interpretive criterion rather than a universal closed-form law: it is sufficient but not necessary for $p^\star = 1$, and its purpose is to identify the structural regime in which the LoS concentration loss dominates any clustered-part FrFT gain.

B. Numerical instantiation for the channel considered

Under the current channel parameterization, the LoS power fraction is approximately $\alpha \approx 0.909$. The two quantities in (16) are evaluated independently of the BER experiment. $\Delta J_{\mathrm{LoS}}(Q)$ is computed from the LoS model in (11): since $J_{\mathrm{LoS}}(1,Q) = 1$ and $\boldsymbol{F}_p \boldsymbol{D}(\nu_0) \boldsymbol{F}_p^H$ spreads energy over $O(N)$ diagonals for $|p-1| > 0.05$, numerical evaluation over $\mathcal{P}$ gives $\Delta J_{\mathrm{LoS}}(3) > 0.50$. $\Delta J_{\mathrm{cl}}(Q)$ is measured on the isolated clustered component $\boldsymbol{H}_{\mathrm{cl}}$ with $\boldsymbol{H}_{\mathrm{LoS}}$ removed, using $M_{\mathrm{sel}} = 60$ pilot realizations drawn with a seed independent of the BER simulation; the measured value is $\Delta J_{\mathrm{cl}}(3) \approx 0.06$. In the notation of (16), this gives

$$\alpha_{\mathrm{th}}(3) < 1 - \frac{0.06}{0.50} = 0.88 < 0.909, \tag{17}$$

confirming $p^\star(3) = 1$, consistent with the BER simulation results.

C. Why the multi-slope structure limits FrFT gain

The clustered component of the channel does not admit a single FrFT-aligned ridge. Even after removal of the LoS contribution, the dominant and secondary clusters follow different effective slopes, approximately κ and 0.55κ. No single FrFT rotation can simultaneously align both structures to the diagonal. Consequently, the term $\Delta J_{\mathrm{cl}}(Q)$ in (16) remains limited, whereas the LoS term continues to favor $p = 1$.

This interpretation differs from the channels in which FrFT-OFDM has often been reported to be beneficial. The issue is therefore not high mobility alone, but the incompatibility of the dominant delay–Doppler slopes seen by a single global transform order.

IV. Validation and Simulation Results

A. Synthetic-operator sanity check

The discrete FrFT implementation and the order-selection rule were checked using synthetic operators with known optimal transform orders: one DFT-diagonal operator ($p_0 = 1$) and two FrFT-diagonal operators ($p_0 = 0.69,\ 1.19$). As shown in Fig. 1, the score $J(p,Q)$ peaks at the design order in each case. This confirms that clear non-DFT optima are recovered when they exist, so the observed collapse to $p^\star \approx 1$ in the NTN channel is not attributable to a DFT-biased implementation or order-selection metric.

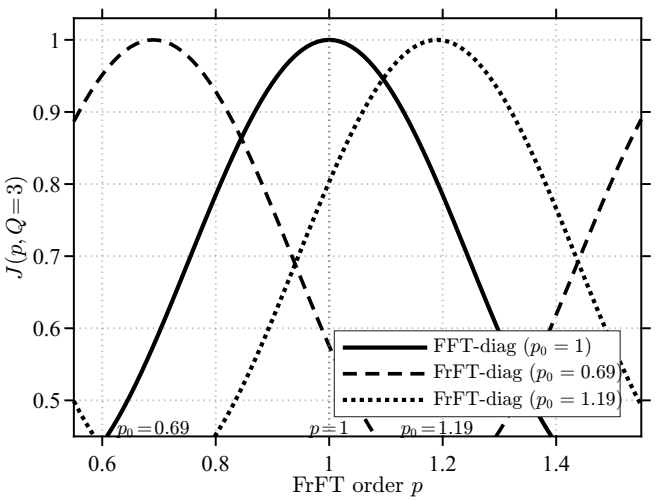

Fig. 1. Synthetic-operator sanity test for $J(p, Q = 3)$. The DFT-diagonal operator is maximized at $p = 1$, whereas the FrFT-diagonal operators are maximized near their design orders $p_0 = 0.69$ and $p_0 = 1.19$. The result indicates that non-DFT optima are recovered when the operator is approximately diagonal in a single FrFT basis.

B. Setup

All numerical results use QPSK, $N = 256$, a PCG banded LMMSE equalizer, and an SNR range from 6 to 20 dB. The transform order is selected independently for each Q using the truncation-aware score described in Section II-A at a fixed selection SNR of 20 dB. Unless otherwise stated, the BER results use $M = 10{,}000$ Monte Carlo realizations.

For the LoS-dominant multi-cluster NTN channel considered here, the ridge-tilt parameter is swept over $\kappa \in \{1000, 1300, 1600\}$ Hz/sample, and two geometry assumptions are considered: INDEP and SHARED. Representative BER plots are reported for $Q \in \{1, 3, 5\}$. Under $M = 10{,}000$ Monte Carlo realizations, the standard deviation of $\log_{10}(\mathrm{BER})$, estimated as $\hat{\sigma} \approx (\mathrm{BER}/M)^{1/2}/\ln 10$, is approximately 0.002–0.003 at the BER levels observed for SNR ≥ 14 dB. Consequently, $|\Delta_{\mathrm{BER}}| \leq 0.01$ lies within two standard deviations of zero, and all values in Fig. 3 satisfy this bound for $Q \geq 1$. To summarize FFT–FrFT performance differences compactly, the quantity

$$\Delta_{\mathrm{BER}}(\kappa, Q) \triangleq \mathrm{median}_{\mathrm{SNR} \geq 14\,\mathrm{dB}} \log_{10} \frac{\mathrm{BER}_{\mathrm{FFT}}(\kappa, Q, \mathrm{SNR})}{\mathrm{BER}_{\mathrm{FrFT}}(\kappa, Q, \mathrm{SNR})} \tag{18}$$

was used. Positive values indicate a BER advantage of FrFT over FFT, negative values indicate an FFT advantage, and values near zero indicate no measurable difference.

C. Representative BER curves

Figure 2 shows BER versus SNR for the LoS-dominant multi-cluster NTN channel with $\kappa = 1300$ Hz/sample under

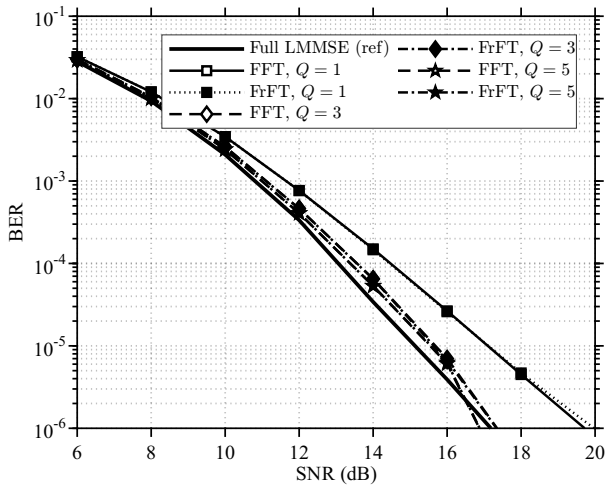

Fig. 2. BER vs. SNR, $\kappa = 1300$ Hz/sample, INDEP geometry. Full LMMSE references coincide (single thick line). Banded results: $Q \in \{1, 3, 5\}$.

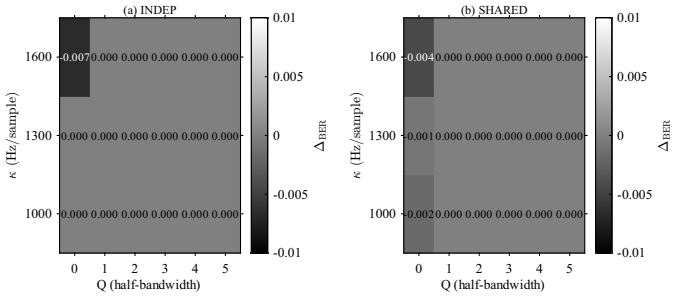

Fig. 3. Summary of $\Delta_{\mathrm{BER}}(\kappa, Q)$ for the LoS-dominant multi-cluster NTN channel over $\kappa \in \{1000, 1300, 1600\}$ Hz/sample and both geometry assumptions. Values near zero indicate no measurable FFT–FrFT difference, whereas negative values indicate a slight FFT advantage.

the INDEP geometry. The full LMMSE FFT and FrFT references coincide and are therefore shown as a single thick reference curve. For $Q \in \{3, 5\}$, the banded FFT and FrFT curves are visually indistinguishable over the full SNR range, implying $\Delta_{\mathrm{BER}}(1300, Q) \approx 0$.

At $Q = 1$, however, the FrFT curve lies slightly above the FFT curve at high SNR. This behavior is consistent with the structural interpretation in Section III: when the optimal order remains very close to unity, a small non-DFT rotation may spread energy away from the single retained diagonal of the narrow-band equalizer, whereas the exact DFT preserves that diagonal concentration.

D. Robustness across κ and geometry

The robustness sweep confirms that the result is not tied to a single parameter point. For $\kappa \in \{1000, 1300, 1600\}$, $\Delta_{\mathrm{BER}}(\kappa, Q) \approx 0$ for all tested combinations with $Q \geq 1$, while a small negative value is observed only at the narrowest bandwidth ($Q = 0$, $\kappa = 1600$). The conclusion is unchanged across the ridge-tilt sweep and across both INDEP and SHARED geometry assumptions.

V. Conclusion

A structural re-examination of FrFT-OFDM in a LoS-dominant multi-cluster NTN channel has been presented. The analysis shows that the optimal FrFT order collapses to the DFT point when the DFT-domain LoS concentration dominates any concentration gain obtainable from the clustered component. In the channel considered here, the dominant and secondary clusters follow incompatible delay–Doppler slopes, so a single FrFT rotation cannot simultaneously align the effective channel to a narrow diagonal band. Under those conditions, FFT-OFDM and FrFT-OFDM are effectively indistinguishable for $Q \geq 2$, with a small penalty emerging only at the narrowest equalization settings ($Q \leq 1$), most pronounced at $Q = 0$ and $\kappa = 1600$ Hz/sample.

The synthetic-operator sanity test indicates that the discrete FrFT implementation can recover clear non-DFT optima when the operator is approximately diagonal in a single FrFT basis. The negative result is therefore interpreted here as a structural property of the LoS-dominant multi-cluster NTN channel rather than as a numerical artefact. The results indicate that the effectiveness of FrFT-OFDM is governed not only by mobility severity, but also by whether the channel admits a single globally alignable ridge. FrFT remains meaningful in single-ridge or weak-LoS settings, but its benefit is absent in multi-cluster NTN channels of the type considered here.

References

[1] 3GPP, "Study on NR to support non-terrestrial networks," Tech. Rep. TR 38.811, Release 17, Jun. 2022.
[2] I. del Portillo, B. G. Cameron, and E. F. Crawley, "A technical comparison of three LEO satellite constellation systems to provide global broadband," *Acta Astronautica*, vol. 159, pp. 216–225, 2019.
[3] L. B. Almeida, "The fractional Fourier transform and time-frequency representations," *IEEE Trans. Signal Process.*, vol. 42, no. 11, pp. 3084–3091, 1994.
[4] M. Martone, "A multicarrier system based on the fractional Fourier transform for time-frequency-selective channels," *IEEE Trans. Commun.*, vol. 49, no. 6, pp. 1011–1020, 2001.
[5] A. Solyman, S. Weiss, and J. J. Soraghan, "Fractional Fourier transform OFDM system performance enhancement over doubly dispersive channels," in *Proc. IEEE GLOBECOM*, 2012.
[6] Z. Mokhtari and M. Sabbaghian, "Near-optimal angle of transform in FrFT-OFDM systems based on channel information," *IEEE Trans. Veh. Technol.*, vol. 67, no. 8, pp. 7663–7668, 2018.
[7] H. Attar *et al.*, "Fractional Fourier transform-based OFDM system with low complexity equalizer for underwater acoustic communications," in *Proc. ACIT*, 2024.
[8] W. Li, Z. Wang, and J. Yu, "Performance improvement by FrFT-OFDM for visible light communication and positioning systems," *Photonics*, vol. 11, no. 12, p. 1147, 2024.
[9] S.-C. Pei and J.-J. Ding, "Closed-form discrete fractional and affine Fourier transforms," *IEEE Trans. Signal Process.*, vol. 48, no. 5, pp. 1338–1353, 2000.
[10] I. Barhumi, G. Leus, and M. Moonen, "Equalization for OFDM over doubly selective channels," *IEEE Trans. Signal Process.*, vol. 54, no. 4, pp. 1445–1458, 2006.
[11] L. Rugini, "Performance analysis of banded equalizers for OFDM systems in time-varying channels," in *Proc. IEEE SPAWC*, 2007.